A Power-Function-Based Hysteresis Modeling Method for Precise Torque Control of Nonlinear Compliant Actuators

Zhou, Libo; Ma, Yuye; Ou, Linlin; Wei, Yan; Bai, Shaoping; Chen, Weihai; Yu, Xinyi

Published in:
IEEE/ASME Transactions on Mechatronics

DOI (link to publication from Publisher):
10.1109/TMECH.2023.3323551

Publication date:
2024

Document Version
Accepted author manuscript, peer reviewed version

A Power-Function Based Hysteresis Modeling Method for Precise Torque Control of Nonlinear Compliant Actuators

Libo Zhou, Yuye Ma, Linlin Ou, Yan Wei, Shaoping Bai, Weihai Chen and Xinyi Yu

***Abstract*—Compliant actuators are suitable for reliable human-robot interaction applications due to their inherent flexibility and safety. However, a limitation of this type of actuators is that nonlinear hysteresis exists especially for those actuators with nonlinear stiffness, which makes accurate system modeling difficult and further degrades force/torque tracking performance. Current hysteresis models are generally developed with black-boxes and the parameters of these models are obtained with optimization algorithms. However, they are applicable to accurate hysteresis modeling only for a specific hysteresis nonlinear curve, lacking the versatility when dealing with nonlinear torque curves with multiple loops at different amplitudes. In this paper, a compliant actuator with nonlinear stiffness is developed and a novel hysteresis modeling method is proposed for the modeling of hysteresis curves with multiple loops, thus a precise torque control of the actuator can be achieved. In our modeling method, a "virtual deformation" concept is defined to linearize the torque curves of the actuator. The torque curves are segmented into ascending, descending and transition sub curves. A novel model based on power-function is designed with the model parameters adjusted to fit the multiple torque curves at different amplitudes. Experimental results show that the root-mean-square-errors (RMSE) of the estimated torque are reduced by 53.1% and 9.4% and the computation cost is reduced by 95.2% and 66.7%, when compared with the nonlinear backlash model (NBM) and the modified Maxwell-Slip based model respectively. Tests of the torque tracking verify the performance of our proposed inverse model.**

***Index Terms*—Compliant actuator, nonlinear hysteresis, multiply loops, torque control, virtual deformation.**

I. INTRODUCTION

COMPLIANT actuators have the advantages of shock tolerance, energy storage, and accurate and stable force control, which are suitable for human-robot interaction applications, such as exoskeletons and prosthesis for human walking assistance [1]-[7]. Compliant actuators allow deviations from its own equilibrium position according to the applied external force. The stiffness of a compliant actuator is comparable with the stiffness of a linear spring. For soft springs, the force fidelity is high but the force bandwidth is limited. On the contrary, for hard springs, there is a wide force range but the force fidelity is decreased [8]. To deal with this inherent contradiction between the force fidelity and magnitude, a type of user-defined compliant actuators with nonlinear stiffness has been proposed. For this type of actuators, the stiffness of the actuator is predefined and varies with the output force/torque. Thus, high force fidelity in the low external load while guaranteeing the force range in high external load can be expected [9]-[14].

A common issue in compliant actuators is hysteresis [14], [15]. Due to the hysteresis effect, relationship between the force and displacement is nonlinear and a lag occurs between the application and removal of a force and its subsequent effect. This hysteresis effect becomes more obvious if the compliant actuator is designed with nonlinear stiffness [14]. If the output torque (or force) of compliant actuators is estimated by conventional methods like fitted-curve or conventional Hooke's law [1], which leaves out of the consideration of the hysteresis effect, the force tracking performance will undoubtedly be degraded.

To address this issue, researchers have proposed many efficacious compensation approaches and mathematical models. These models can generally be divided into operator-based models and differential-based models [16]. Operator-based models construct hysteresis models by weighted stacking nonlinear operators. Some classical models include Preisach model, Prandtl-Ishlinskii model, Krasnosel'skii-Pokrovskii model, Maxwell-Slip model and related improved models [17]. The operator-based hysteresis models have high modeling accuracy and are easy to construct their inverse models. However, this modeling methods require a large number of parameters. Differential-based models characterize the hysteresis through constructing differential equations, typical models include Duhem model, Bouc-Wen model and Backlash-Like model [17], [18]. This type of models has simple structure and calculation process. However, the modeling accuracy is limited. Current hysteresis models are usually designed with black-boxes and the parameter values are usually obtained by least mean method, Kalman filter or black box identification methods such as neural network and fuzzy support vector machine [19]. Although high modeling accuracy can be achieved in specific hysteresis nonlinear curve by optimizing the parameter values, a limitation of these methods is the versatility in different hysteresis nonlinear curves with multiply loops [20].

Existing hysteresis models have been successfully applied in the area of smart materials and conventional materials like piezoelectric ceramics actuators and shape memory alloy [21]-[27]. Due to the relatively inconspicuous but complex hysteresis, there are fewer hysteresis modeling methods for motor driven compliant actuators with nonlinear stiffness. In [28], a

This work was supported in part by Zhejiang Provincial Natural Science Foundation of China under Grant No. LQ22F030021, in part by National Natural Science Foundation of China under Grant 62303415, Grant 62373329 and Grant 62203392, and in part by Zhejiang Provincial Natural Science Foundation of China under Grant No. LY21F030018. (Corresponding authors: Weihai Chen and Xinyi Yu)

Libo Zhou, Yuye Ma, Linlin Ou, Yan Wei and Xinyi Yu are with the College of Information Engineering, Zhejiang University of Technology, Hangzhou, 310023, China (e-mail: libozhou@zjut.edu.cn; 2112103326@zjut.edu.cn; linlinou@zjut.edu.cn; weiyanok@zjut.edu.cn; yuxy@zjut.edu.cn).

Shaoping Bai is with the Department of Materials and Production, Aalborg University, Aalborg 9220, Denmark (e-mail: shb@mp.aau.dk).

Weihai Chen is with the School of Automation Science and Electrical Engineering, Beihang University, BJ 100191, China (e-mail: whchen@buaa.edu.cn).

nonlinear backlash model (NBM) based on classical backlash model was proposed to describe the hysteresis curves of a series elastic actuator. In this model, two nonlinear polynomials were used to characterize the ascending and descending curves, and a line with a constant slope was used to characterize the transition curve. However, NBM fails to simulate hysteresis curves for different maximum torques. To deal with this problem, a hysteresis model based on NBM was proposed in [29]. In this model, the hysteresis curve was divided into three parts: loading, transition and unloading. A third-order polynomial was used to simulate the loading curve, an exponential function was used to simulate the unloading curve and a straight line with a constant slope was used to model the transition curve. This model can simulate the hysteresis curves with different amounts of maximum torque. However, the modeling accuracy is reduced in the transition part as the curves in the transition part is a curve rather a straight line. Besides, the inverse hysteresis model is difficult to be constructed due to the use of complicated exponential function. To solve the above problems, a Maxwell-slip based hysteresis modeling method was proposed for a nonlinear compliant actuator in our previous works [30], [31]. In the method, a concept called virtual deformation was adopted to transform the nonlinearity curve into a polyline-based model. Two polynomials were used to simulate the loading and unloading curves and a modified Maxwell-slip model was developed to simulate the transition curves. This model has a high modeling accuracy with a low computation cost. However, the torque curves are considered to have the same slope in the transition curves at different amplitudes, which degrades the modeling accuracy since the slopes are different at different amplitudes. Besides, the computation cost still has to be reduced.

In this paper, a modified nonlinear compliant actuator using tension spring is proposed on the basis of the original design in our previous works [30], [31]. Compared with the previous design, tension spring is used instead of compression spring, which avoids the instability problem of the compression spring. Thus, there is no requirement in the installation of a guide shaft inside the spring to improve its stability, which reduces the friction force between the spring and the guide shaft and the stability is guaranteed during rotation. The torque curves of the developed compliant actuator according to the rotation deformation angle are shown in Fig. 1. Although the hysteresis is reduced compared with our previous design [31], it can be observed that the hysteresis effect is still obvious. Besides, we can find that the torque curves are different with multiply loops, especially in the transition part as magnified shown in Fig. 1 (b), which can be found that the slopes of the curves are different at different amplitudes and are similar to the shapes of power function with different power exponents. If the torque curves with hysteresis are not accurately modeled and compensated at different amplitudes, the torque tracking performance will inevitably be degraded.

In this paper, a "virtual deformation" concept is adopted to alleviate the effects of the nonlinearity caused by the developed mechanism. A modeling method based on power-function with variable-arguments is developed to simulate the torque curves with multiple loops. The proposed hysteresis model is developed with clear and concise architecture and is easy to construct its inverse, which facilitates the development of hysteresis compensator [32].

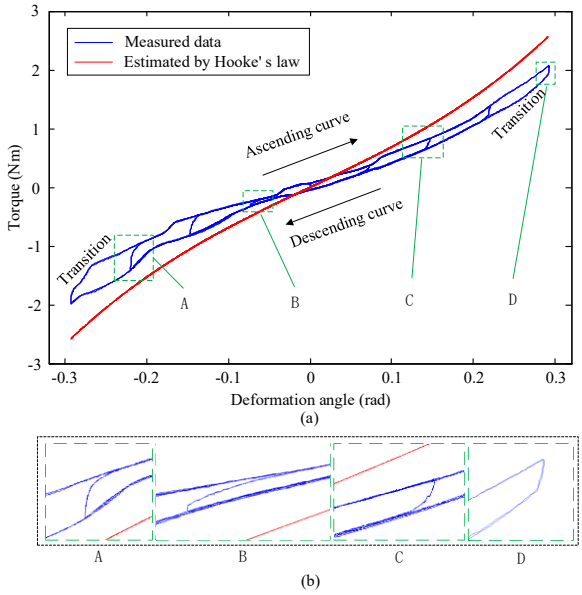

Fig. 1. Multi-loop torque curves of the compliant actuator. (a) Whole trajectories. (b) Magnified four parts of trajectory curves in Transition part.

The rest of this paper is organized as follows. System design of the compliant actuator is described in Section II. A hysteresis modeling method based on power-function is developed in section III. In Section IV, inverse of the proposed hysteresis model is presented. Experimental setup together with the results is presented in Section V. Discussion and Conclusion are included in Sections VI and VII.

II. System Design of the Compliant Actuator

The mechanical model of the actuator together with the platform for tests is shown in Fig. 2. It includes an electrical motor, an input frame, the proposed compliant actuator and a force/torque sensor. In the compliant actuator, a pair of gears (the size ratio of the two gears is 2:1) is used to transport the rotation of the input frame into transition of the transmission rod, thus the two identical tension springs will be stretched or released when the input frame rotates. In the design, a pair of slide guide rails is used to guide the direction and ease the friction of the transmission rod.

The working principle of the actuator is shown in Fig. 3. When the input frame rotates at an angle θ_1, the tension spring is stretched by a distance Δl, which is

$$\Delta l = 2r(1 - \cos\theta_1) \tag{1}$$

where r is the pinion radius.

The tension spring force using Hook's law is

$$F_d = K\Delta l + P_0 \tag{2}$$

where K is the stiffness of the tension spring. P_0 is the pretightening force at initial state shown in Fig. 3 (a).

The tension spring force on the pinion will generate a torque, which can be calculated as

$$\tau_s = F_d r \sin\theta_1 \tag{3}$$

As the diameter of the gear ring is two times of the pinion, the torque transferred to the output plate is magnified by two times. The output torque is calculated as

$$\tau = 2\tau_s \tag{4}$$

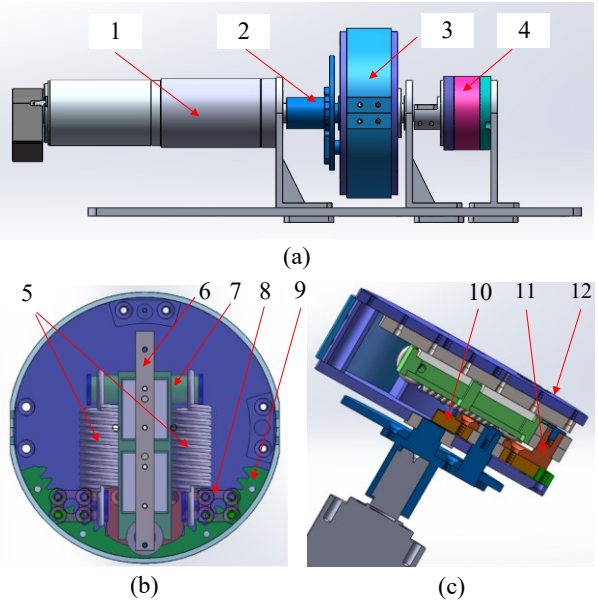

Fig. 2. Mechanical model of the actuator. (a) Overall structure, (b) planar view, (c) section view. 1- Motor, 2-Input frame, 3-Compliant actuator, 4-Force/Torque sensor, 5-Tension spring, 6-Slide guide rails, 7-Transmission rod, 8-Spring retainer, 9-Gear, 10-Pinion, 11-Passing component, 12- Output plate.

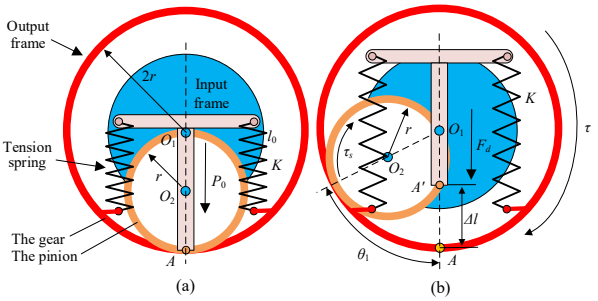

Fig. 3. A schematic diagram of the actuator. (a) initial state, (b) operating state.

Combining (1)-(4), we can get the output torque as

$$\tau = 4Kr^2 \sin\theta_1 (1 - \cos\theta_1) + 2P_0\, r\sin\theta_1 \qquad (5)$$

The theoretical curve is the red curve shown in Fig. 1(a), comparing with the curve measured. It can be seen the curve measured is significantly different from the theoretical one, due the presence of hysteresis, which has to be modeled properly.

III. HYSTERESIS MODELING

A. *Power-function type model*

Our proposed hysteresis modeling method is based on a power-function type model. Prior to introduce our proposed hysteresis modeling method, the power-function type model is briefly described for completeness. Mathematically, a power function is written as

$$y = \beta x^{\alpha} \qquad (6)$$

A few examples of power functions are shown in Fig. 4. It can be found that the curves are similar with the torque curves in Transition part as shown in Fig. 1, and the shapes can be adjusted with different parameters α and β. This provides the possibility of using this type of model to simulate the hysteresis curves with multiple loops.

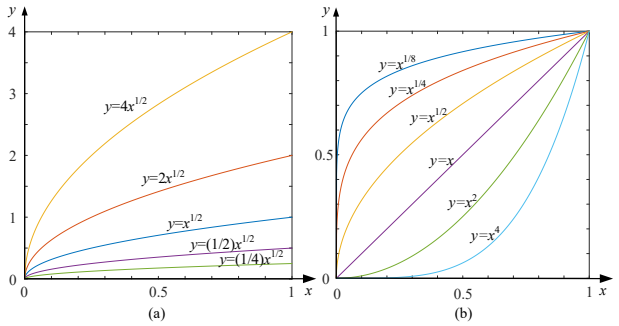

Fig. 4. Examples of power functions. (a) Power functions with different coefficients β. (b) Powers function with different power exponents α.

B. *Proposed power-function based hysteresis model*

In our proposed hysteresis modeling method, a "virtual deformation" is defined to eliminate the nonlinearity effects caused by the proposed mechanism.

According to Eq. (5), the equation of output torque can be rewritten as

$$\tau = K[4r^2 \sin\theta_1 (1 - \cos\theta_1) + \frac{2P_0 r\sin\theta_1}{K}] \qquad (7)$$

A virtual deformation s is defined as

$$s = 4r^2 \sin\theta_1 (1 - \cos\theta_1) + \frac{2P_0 r\sin\theta_1}{K} \qquad (8)$$

Referring to (7) and (8), we can get $\tau = Ks$. Since the values of K is a constant, τ and s are linearly dependent, which shows that the nonlinearity caused by the mechanism rotation is eliminated. Fig. 5 shows the torque curves with respect to the virtual deformation s, which can be found that the ascending and descending curves are straightened.

The proposed hysteresis model is shown in Fig. 6. The trajectories are divided by different line segments by calibrating different position points (A, B, C, $\cdots$), and the hysteresis torque is

$$\tau_{hys} = \begin{cases} \tau_{al}(s), & if\ \ \dot{s} > 0, \text{and}\ \ s > s_{01} \\ \tau_{dl}(s), & if\ \ \dot{s} > 0, \text{and}\ s < s_{02} \\ \tau_{tl}(s), & if\ \ s \le s_{01}, \text{and}\ s \ge s_{02} \end{cases} \qquad (9)$$

where τ_{al}, τ_{dl} and τ_{tl} are the functions for ascending, descending and transition sub curves respectively. s_{01} and s_{02} are the turning points of the transition curve with ascending and descending sub curves, which are updated in real time.

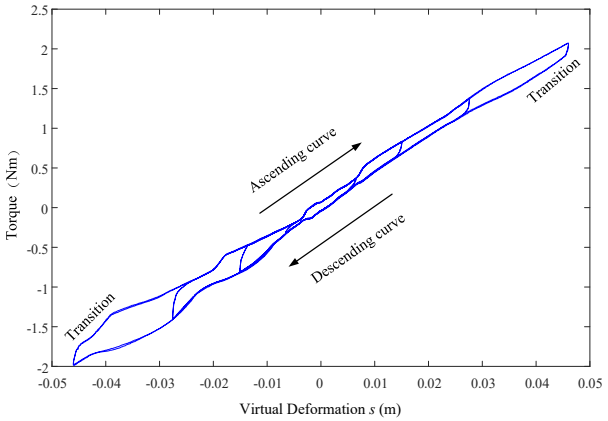

Fig. 5. Torque curves relating to the virtual deformation.

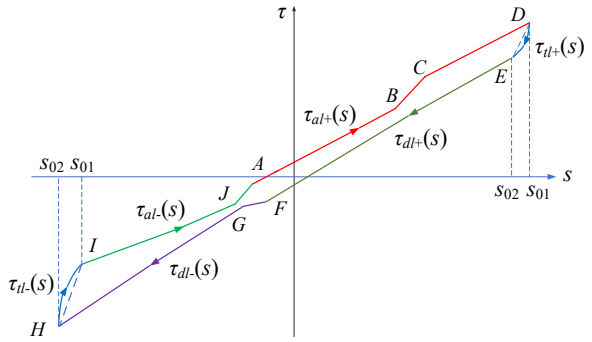

Fig. 6. Illustrations for the proposed model.

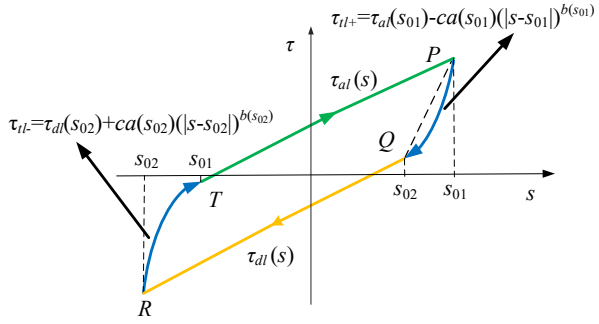

Fig. 7. Illustrations of the power-function based model for transition lines.

The values of s_{01} and s_{02} will be calculated once one of them is given

$$\begin{aligned} s_{01} &= s_{02} + \Delta s_2(s_{02}) \\ s_{02} &= s_{01} - \Delta s_1(s_{01}) \end{aligned} \tag{10}$$

where

$$\begin{aligned} \Delta s_1(s_{01}) &= k_{11}s_{01} + k_{01} \\ \Delta s_2(s_{02}) &= k_{12}s_{02} + k_{02} \end{aligned} \tag{11}$$

where k_{ij}, $i = 0, 1$ and $j = 1, 2$ are constants.

For the turning point s_{01}, it is updated to the value of s when it satisfies the following requirements:

$$\begin{cases} s - s_- > 0 \\ s - s_+ > 0 \\ s - s_{01} > 0 \end{cases} \tag{12}$$

For the turning point s_{02}, it is updated to the value of s when it satisfies:

$$\begin{cases} s - s_- < 0 \\ s - s_+ < 0 \\ s - s_{02} < 0 \end{cases} \tag{13}$$

where s_- and s_+ are the previous and next point of s, respectively.

For ascending and descending curves, the torque functions can be written in detail as

$$\tau_{al}(s) = k_{ij}(s - s_i), \qquad \text{if } s \in [s_i, s_j] \tag{14}$$

$$\tau_{dl}(s) = k_{pq}(s - s_p), \qquad \text{if } s \in [s_p, s_q] \tag{15}$$

where $k_{ij} = \frac{\tau_j - \tau_i}{s_j - s_i}$ (i, j=A, B, C, D, I, J), $k_{pq} = \frac{\tau_q - \tau_p}{s_q - s_p}$ (p, q=H, G, F, E). As shown in Fig. 6, i and j, p and q indicate two adjacent points, k_{ij} and k_{pq} refer to the slopes of a certain segment in the ascending and descending curves, respectively. τ_i and s_i are coordinate of point i.

For transition curves, it is modeled by a power function-based model as shown in Fig. 7, which can be described as

$$\tau_{tl}(s) = \begin{cases} \tau_{dl}(s_{02}) + f(s - s_{02}), & \text{if } \dot{s} > 0 \\ \tau_{al}(s_{01}) - f(s - s_{01}), & \text{if } \dot{s} < 0 \end{cases} \tag{16}$$

$$f(s - s_{0i}) = ca(s_{0i})(|s - s_{0i}|)^{b(s_{0i})} \qquad i = 1, 2 \tag{17}$$

where c is a variable defined in (19).

Referring to Fig. 4, we can get that by setting different values of a and b, the torque covers will be adjusted. Thus, appropriate values of a and b can be selected with the help of Curve Fitting Toolbox in Matlab software to fit the torque curves in transition segment at different amplitudes. The values of a and b with different amplitudes are obtained as

$$\begin{aligned} a(s_{0i}) &= p_{2i}{s_{0i}}^2 + p_{1i}s_{0i} + p_{0i} \\ b(s_{0i}) &= g_{2i}{s_{0i}}^2 + g_{1i}s_{0i} + g_{0i} \end{aligned} \qquad i = 1, 2 \tag{18}$$

where p_{ji} and g_{ji} are constants, j=0, 1, 2, i = 1, 2.

To ensure a smooth connection of the transition curve with ascending and descending curves, parameter c of (17) is determined by

$$c = \frac{\tau_{al}(s_{01}) - \tau_{dl}(s_{02})}{a(s_{0i})(|s_{01} - s_{02}|)^{b(s_{0i})}} \tag{19}$$

IV. Inverse Hysteresis Modeling

To mitigate the hysteresis effect on the torque control of actuators, a simple and effective way is to construct a feedforward inverse compensator [32]. To build this hysteresis compensator, the inverse of the hysteresis model is necessary to be constructed accurately.

An illustration for the proposed inverse hysteresis model is seen in Fig. 8. In the inverse model, the input and output are the reference torque and the virtual deformation respectively. Referring to Figs. 6 and 8, we can find that the difference between the proposed hysteresis model and its inverse is that the abscissa and ordinate values are switched. The virtual deformation s is

$$s = \begin{cases} S_{al}(\tau), & if\ \ \dot{\tau} > 0, and\ \ \tau > \tau_{01} \\ S_{dl}(\tau), & if\ \ \dot{\tau} > 0, and\ \tau < \tau_{02} \\ S_{tl}(\tau), & if\ \ \tau \le \tau_{01}, \text{and } \tau \ge \tau_{02} \end{cases} \tag{20}$$

where S_{al}, S_{dl}, S_{tl} are the functions for ascending, descending lines and transition sub curves respectively. τ_{01} and τ_{02} are the turning points of the transition curve with ascending and descending curves, which are updated in real time.

The values of τ_{01} and τ_{02} are calculated once one of them is given

$$\begin{aligned} \tau_{01} &= \tau_{02} + \Delta\tau_2(\tau_{02}) \\ \tau_{02} &= \tau_{01} - \Delta\tau_1(\tau_{01}) \end{aligned} \tag{21}$$

with

$$\begin{aligned} \Delta\tau_1(\tau_{01}) &= l_{11}\tau_{01} + l_{01} \\ \Delta\tau_2(\tau_{02}) &= l_{12}\tau_{02} + l_{02} \end{aligned} \tag{22}$$

where l_{ij}, $i = 0, 1$ and $j = 1, 2$ are constants.

For the turning point τ_{01}, it is updated to the value of τ when it satisfies the following requirements:

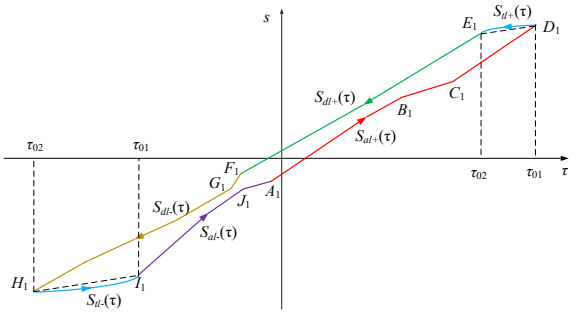

Fig. 8. Illustrations for the inverse hysteresis model. τ_{01} and τ_{02} correspond to s_{01} and s_{02}, A_1, B_1, $\cdots$ J_1 correspond to A, B, $\cdots J$ in Fig. 5. The abscissa and ordinate values of A_1 and A are opposite, the same for B_1, $\cdots$ J_1.

$$\begin{cases} \tau - \tau_- > 0 \\ \tau - \tau_+ > 0 \\ \tau - \tau_{01} > 0 \end{cases} \tag{23}$$

For the turning point τ_{02}, it is updated to the value of τ when it satisfies:

$$\begin{cases} \tau - \tau_- < 0 \\ \tau - \tau_+ < 0 \\ \tau - \tau_{02} < 0 \end{cases} \tag{24}$$

For ascending and descending curves, the functions can be described in detail as

$$S_{al}(\tau) = l_{ij}(\tau - \tau_i), \qquad \text{if } \tau \in [\tau_i, \tau_j] \tag{25}$$

$$S_{dl}(\tau) = l_{pq}(\tau - \tau_p), \qquad \text{if } \tau \in [\tau_p, \tau_q] \tag{26}$$

where $l_{ij} = \frac{s_j - s_i}{\tau_j - \tau_i}$ (i, j=A_1, B_1, C_1, D_1, I_1, J_1), $l_{pq} = \frac{s_q - s_p}{\tau_q - \tau_p}$ (p, q=H_1, G_1, F_1, E_1). As shown in Fig. 8, i and j, p and q are two adjacent points, l_{ij} and l_{pq} refer to the slopes of a certain segment in the ascending and descending curves, respectively. τ_i and s_i are coordinate values of point i.

For transition curves, it is modeled by

$$s_{tl}(s) = \begin{cases} s_{dl}(\tau_{02}) + g(\tau - \tau_{02}), & \text{if } \dot{s} > 0 \\ s_{al}(\tau_{01}) - g(\tau - \tau_{01}), & \text{if } \dot{s} < 0 \end{cases} \tag{27}$$

Since the ordinate and abscissa values are switched in the inverse model, referring to (16) and (17), we set

$$g(\tau - \tau_{0i}) = \frac{h}{a(\tau_{0i})}(\tau - \tau_{0i})^{\frac{1}{b(\tau_{0i})}} \quad i = 1, 2 \tag{28}$$

where h is a variable defined in (31), and the values of a and b are obtained as

$$\begin{aligned} a(\tau_{0i}) &= p_{2i}S(\tau_{0i})^2 + p_{1i}S(\tau_{0i}) + p_{0i} \\ b(\tau_{0i}) &= g_{2i}S(\tau_{0i})^2 + g_{1i}S(\tau_{0i}) + g_{0i} \end{aligned} \quad i = 1, 2 \tag{29}$$

$$S(\tau_{0i}) = \begin{cases} S_{al}(\tau_{01}), & i = 1 \\ S_{dl}(\tau_{02}), & i = 2 \end{cases} \tag{30}$$

where p_{ji} and g_{ji} are constants, j=0, 1, 2, i = 1, 2.

For the value of h, it is used to ensure a smooth connection of the transition curve with ascending and descending curves, which is obtained by

$$h = \frac{a_i(\tau_{0i})[S_{al}(\tau_{01}) - S_{dl}(\tau_{02})]}{(|s_{01} - s_{02}|)^{\frac{1}{b_i(\tau_{0i})}}} \tag{31}$$

The working procedure of the inverse hysteresis model is similar with the original hysteresis model described in Section III. It is noted that most of the parameters of the inverse hysteresis model can be got directly by conversion of the proposed hysteresis model. This simplifies the inverse hysteresis modeling process and improves the hysteresis compensation effect.

With the above inverse hysteresis model, the virtual deformation s can be obtained when the reference torque trajectory is given. Then, the reference angle trajectory θ_r for the motor can be calculated by constructing the inverse kinematics equation of s according to (8).

V. Experiments

A prototype of the actuator in Fig. 2 was developed for testing purpose and its main parameters are listed in Table I. The experimental platform as shown in Fig. 9 includes the compliant actuator, a motor driven system, a Force/Torque sensor and a host computer. In the experiments, a 500 CPT encoder mounted on the motor was used to measure the rotation angle of the compliant actuator and a Force/Torque sensor (MINI 45, ATI) with a resolution of 1/1504 Nm was set up on the output plate for measuring the output torque of the compliant actuator. The sampling frequency is 100 Hz in the experiments. A user interface was developed in the host computer for high level operation. The data of the measured rotation angle, output torque and the current running time was saved in the host computer.

TABLE I
The Main Dimension Parameters of the Compliant Actuator

Item	Compliant Actuator
Stiffness of the tension spring K	15.49 N/mm
Initial length of the tension spring	55 mm
Radius of the pinion r	21 mm
Range of deformation angle θ_1	-0.5~0.5 rad
Dimension (diameter × thickness)	100 × 35 mm^2
Weight (without driven motor)	about 0.45 kg

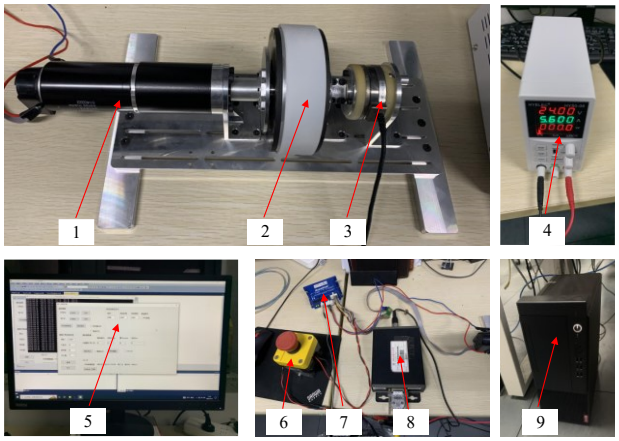

Fig. 9. Experimental platform. 1-Maxon Motor RE40, 2-Actuator prototype, 3-ATI Force/Torque sensor, 4-Power supply, 5-User interface, 6-Emergency stop, 7-Copley motor drive, 8-Data collection system of ATI sensor, 9-Host computer.

A. *Construction and validation of the hysteresis model*

In the experiments, the output torque and the rotation angle of the actuator were measured. Then, the curves of the output torque with respect to the virtual deformation are obtained. By calibrating the key points in the figures (Seen in Figures 22 and 23), the parameters can be obtained. The values of the parameters used in the experiments are listed in Tables V and VI in Appendix. The estimated torque by the proposed hysteresis model together with the output torque measured is shown in Figs. 10 and 11. We can find that the errors between them are less than 0.02 Nm in general, which show that the proposed hysteresis model has a high modeling accuracy of nonlinear torque curves with multiple loops.

The program codes of NBM [28], Modified Maxwell-slip based model [31] and the proposed model are generated by Matlab software and running on the host computer. The root-mean-square-errors (RMSE) and maximum errors between the estimates and measured are then calculated. Besides, the computation cost defined by the whole running time of the program is obtained.

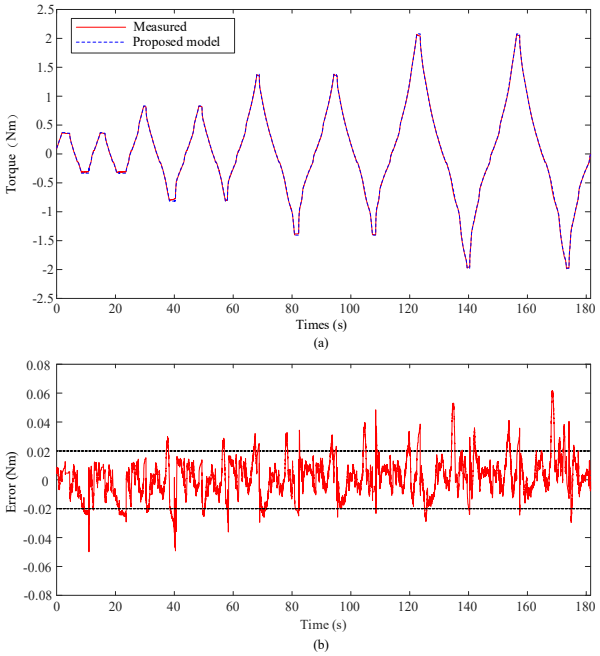

Fig. 10. Torque measurement and estimation by the proposed model. (a) torques, (b) plot of errors.

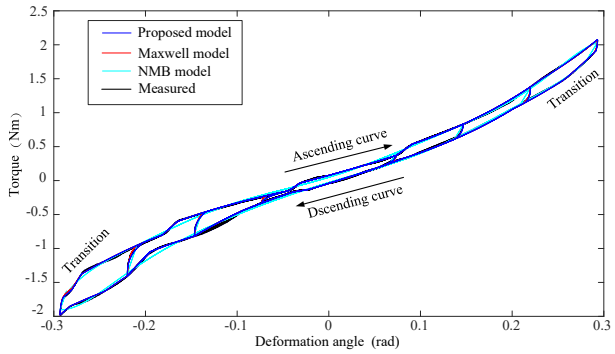

Fig. 11. Torque measurement and estimate by the proposed model via deformation angles.

TABLE II
ERROR COMPARISON OF THE TORQUE MEASUREMENT METHODS

Hysteresis model	RMSE (Nm)	Max. error (Nm)	Com. cost (s)
NBM	0.0288	0.247	0.021
Max. based model	0.0149	0.0975	0.003
Proposed model	0.0135	0.0612	0.001

Experimental results using the above three models are shown in Table II. Compared with the NBM and Maxwell-slip based model, the RMSE are reduced by 53.1% and 9.4%, and the computation cost are reduced by 95.2% and 66.7%, respectively.

B. *Experiments with the inverse hysteresis model*

Inverse of the proposed model, NBM and the modified Maxwell-slip based model are developed to test the performance of our proposed modeling method. The RMSE and maximum errors between the measured results and estimates are calculated and the computation cost is acquired. Experimental results by the proposed hysteresis model are shown in Figs. 12 and 13. It is seen that the errors are less than 0.004 rad in most period.

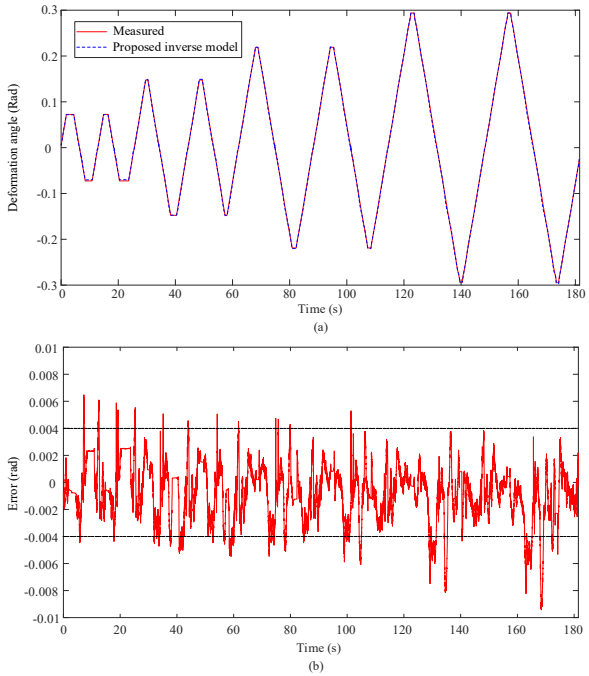

Fig. 12. Deformation measurements and estimation by the proposed inverse model. (a) torques, (b) plot of errors.

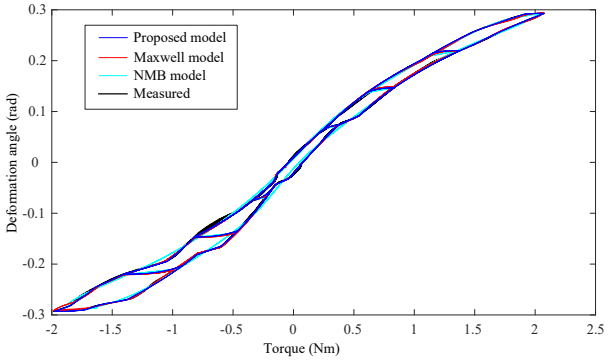

Fig. 13. Deformation measurements and estimates by the proposed inverse model via different torque amplitudes.

TABLE III
ERROR COMPARISON OF ANGLE MEASUREMENT METHODS

Hysteresis model	RMSE (rad)	Max. error (rad)	Com. cost (s)
Inv. NBM	0.0076	0.044	0.081
Inv. Max. model	0.0030	0.011	0.013
Prop. Inv. Model	0.0023	0.009	0.009

Statistical results using the above three inverse models are listed in Table III. Compared with inverse NBM and inverse Maxwell-slip based model, the RMSE is reduced by 69.7% and 23.3%, and the computation cost is reduced by 88.9% and 30.8%, respectively. These results verify that our proposed inverse hysteresis model has a high modeling accuracy with a low computation cost for nonlinear curves with multiple loops.

C. *Experiments of the torque tracking*

To verify the torque tracking performance of the proposed compliant actuator with our proposed hysteresis modeling method, experiments with three different sinusoidal torque trajectories were conducted. Upon the proposed inverse hysteresis model, the inverse of the modified Maxwell-slip based model and the inverse NBM, the reference deformation angle trajectories of the compliant actuator were obtained. Then, the compliant actuator would rotate in accordance with the reference rotation angle trajectories for torque tracking under the controller shown in Fig. 14. In the controller, the proposed hysteresis model is used for precorrection.

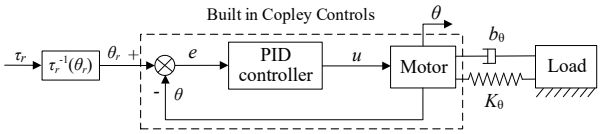

Fig. 14. Control diagram of the actuator for torque tracking.

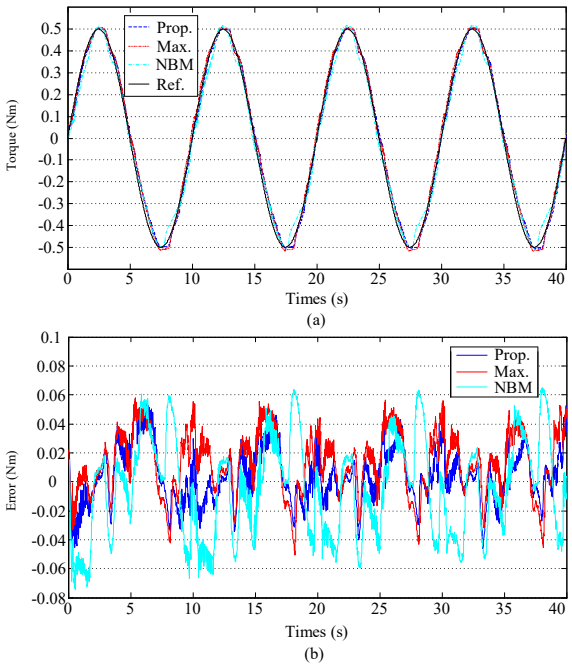

Fig. 15. Torque tracking results under reference: $\tau = 0.5\sin(0.2\pi t)$ Nm. (a) torques, (b) plot of errors.

Results of the torque tracking experiments are shown in Figs. 15-17 and the statistical data is listed in Table IV. It can be seen that the errors between the measured and the reference torques are minimum by our proposed hysteresis model. The RMSE is reduced by 7.4% - 26.9% and 38.1%-44.1% and the maximum error is reduced by 8.6%-18.4% and 26.1%-41.1% with three different amplitudes compared with the modified Maxwell-slip based model and NBM, respectively.

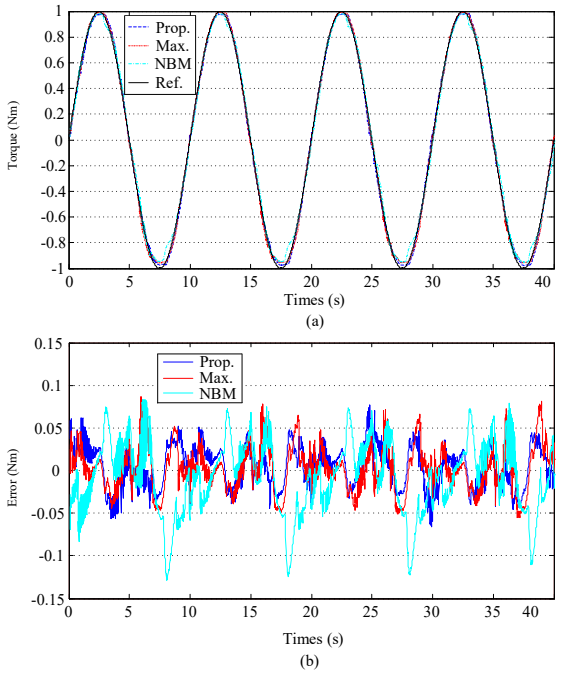

Fig. 16. Torque tracking results under reference: $\tau = \sin(0.2\pi t)$Nm. (a) torques, (b) plot of errors.

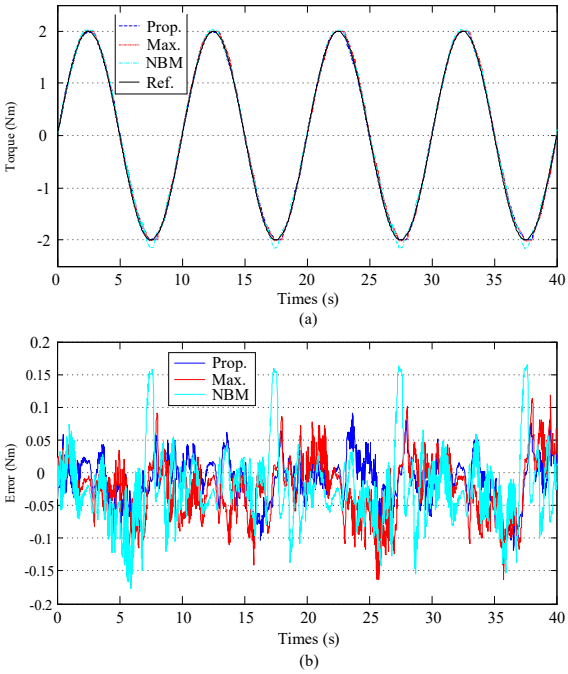

Fig. 17. Torque tracking results under reference: $\tau = 2\sin(0.2\pi t)$Nm. (a) torques, (b) plot of errors.

TABLE IV
TORQUE TRACKING ERRORS

Torque magnitude	Hysteresis model	RMSE (Nm)	Max. error (Nm)
0.5 Nm	NBM	0.034	0.074
	Max.	0.025	0.058
	Prop.	0.019	0.053
1 Nm	NBM	0.042	0.129
	Max.	0.027	0.086
	Prop.	0.025	0.076
2 Nm	NBM	0.063	0.180
	Max.	0.052	0.163
	Prop.	0.039	0.133

VI. DISCUSSION

The force/torque tracking problem can be converted into position tracking problem by using compliant actuators, which simplifies the complexity of force/torque tracking controller. A limitation of this type of actuators is the force fidelity and the force bandwidth cannot be satisfied simultaneously. To solve the above problem, a novel compact compliant actuator with nonlinear stiffness is proposed. The stiffness of the actuator can be varied according to the extern load. When the extern load is small, the actuator is soft, and the stiffness will increase with the increase of the extern load. Therefore, the proposed actuator can realize both high force fidelity and large force generation.

Due to friction, material deformation and clearance between the mechanism parts, the hysteresis effect is obvious and the torque curves are nonlinear and vary with amplitudes in nonlinear compliant actuators. This makes the hysteresis effect difficult to be accurately compensated, which will decrease the torque tracking performance. To overcome this issue, the design of a hysteresis model with high modeling accuracy and lower computation cost is necessary. With our proposed hysteresis modeling method, a significant improvement in force/torque tracking performance of compliant actuators can be expected.

Conventional mathematical models of hysteresis, like the Bouc-Wen model, Prandtl-Ishlinskii model and Maxwell-Slip model, are usually designed with black-boxes and the parameter values are usually obtained by least mean method, Kalman filter or black box identification methods. Although high modeling accuracy can be achieved in specific hysteresis nonlinear curve by optimizing the parameter values, a limitation of these methods is the versatility in different hysteresis nonlinear curves with multiply loops. As the torque curves of nonlinear compliant actuators vary with amplitudes, it is quite difficult to turn the model parameters to match the experimental data well among inputs with different amplitudes. In our proposed model, the torque curves are segmented into ascending, descending and transition sub curves by the turning points s_{01} and s_{02}. Thus, the trajectory curves in the three parts are decoupled. Two polynomials are then used to simulate the ascending and descending curves and a power-function based model with adjustable parameters is developed to simulate the transition curves. Results verified that the model can simulate the torque curves accurately with multiple loops.

It is noted that there is a set of parameters with constants used in our model. Fortunately, the values of the parameters can be obtained manually with simple operation. For example, the parameters of l_{ij} and l_{pq}, by calibrating several key points as shown in Fig. 22 in Appendix, the parameters can then be obtained according to (14) and (15).

To show the versatility of the proposed model in different scenarios, experiments of the torque trajectories with different shapes were conducted. The results using the proposed model are shown in Fig. 18. It can be found that there is no significant difference on the modeling accuracy of the torque curves with different shapes.

In the proposed model, the influence of signal frequency has not been considered. To show the possible influence of the frequency on the modeling accuracy, experimental results of the actuator with the frequency from 0.035 Hz to 1 Hz are included. As shown in Fig. 19, there is no significant difference on the modeling accuracy, of course, the errors are slightly increased with the frequencies.

The potential application of the proposed compliant actuator is wearable robots. A lower limb exoskeleton driven by the proposed compliant actuator has been designed as shown in Fig. 20. The size and spring stiffness of the compliant actuator can be adjusted to satisfy the torque and size requirements of the exoskeleton. It is noted that the torque curves with hysteresis is affected by the external disturbance [33], which is inevitable in exoskeleton robot applications. In our proposed model, the external disturbance is not considered at present. To overcome this problem, a controller considering the external disturbance (from the load of the actuator) is proposed for future implementation, as shown in Fig. 21. A feedforward controller considering the deflection angle $(\theta_1 - \theta_2)$, rotation angle θ_2 and rotation speed $\dot{\theta}_2$ of the load will be developed to compensate the influence of the external disturbance from the load.

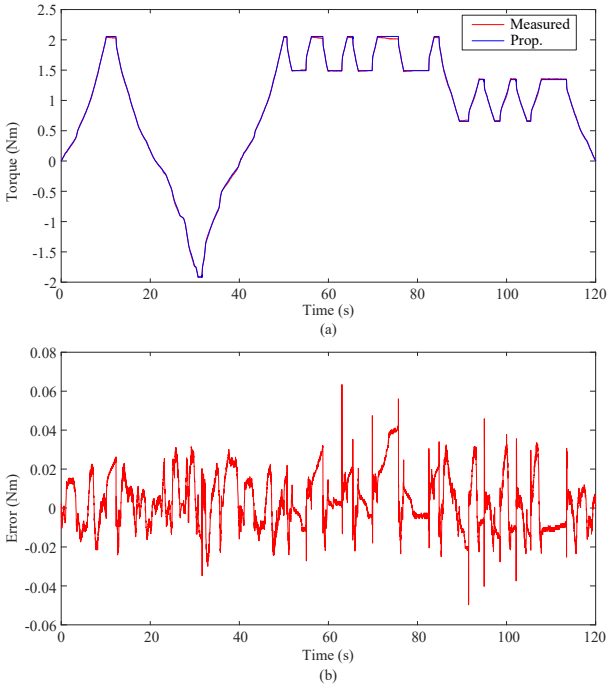

Fig. 18. Torque measurements and estimates by the proposed model with different torque curves. (a) torques, (b) plot of errors.

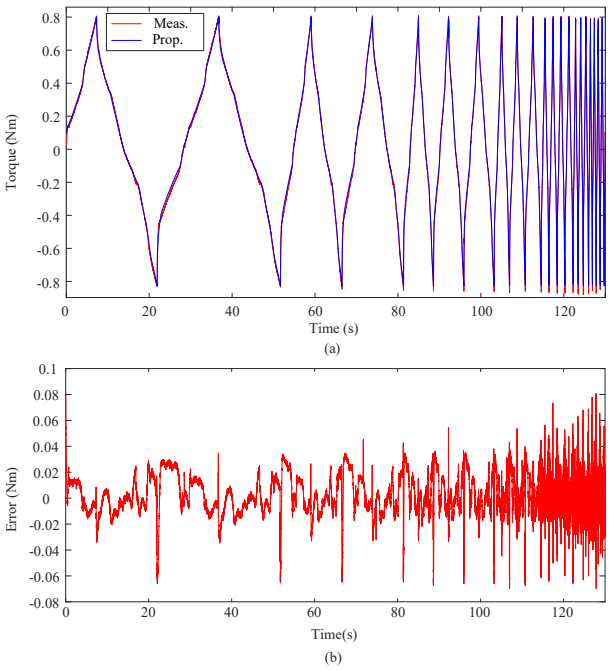

Fig. 19. Torque measurements and estimates by the proposed model with different frequencies. (a) torques, (b) plot of errors.

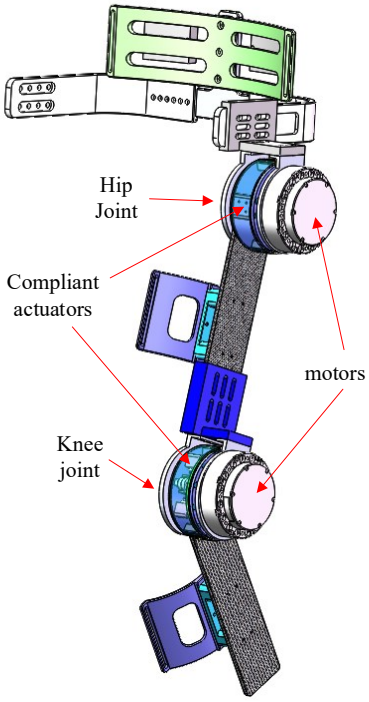

Fig. 20. A lower limb exoskeleton driven by the compliant actuator.

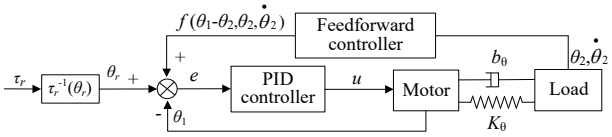

Fig. 21. Control strategy for the compensation of the external disturbance from the load.

VII. Conclusion

In this paper, a nonlinear compliant actuator was presented. The design and working principle of the actuator was described. A power-function based hysteresis model and its inverse model were developed. A prototype of the compliant actuator was constructed and experimental results verified that the proposed hysteresis model has a high modeling accuracy and a low computation cost.

A major contribution of this work is the hysteresis modeling for a nonlinear compliant actuator, which has nonlinear torque curves with multiply loops at different amplitudes. In our modeling method, a "virtual deformation" concept was introduced to linearize the torque curves of the compliant actuator. Then, a power-function based hysteresis model was developed to model the nonlinear torque curves accurately with multiply loops at different amplitudes. Experimental results show that both high modeling accuracy and lower computation cost are reached in our proposed hysteresis model. Construction of the inverse hysteresis model is similar with the original model and a hysteresis compensator is convenient to be designed.

Another contribution of this work lies in the modification of the compliant actuator. In our new design, a tension spring-based mechanism is used instead of the compression spring-based mechanism, which reduces the friction force and improve the stability during rotation. The hysteresis of this new actuator is significantly decreased compared with our original design [31]. Future work will focus on the compensation of the external disturbance. Besides, applications of the compliant actuator in a lower limb exoskeleton robot will be further investigated.

Appendix

To show the values of the key parameters in the proposed model used in the experiments, the torque trajectories with the calibration points are shown in Fig. 22 and listed in Table V. Then the parameters k_{ij} and k_{pq} can then be obtained according to (14) and (15).

For the parameter values in (11), the values of Δs_1 and Δs_2 will first defined manually with different turning points s_{01} and s_{02}. then, a linear function shown in (11) are used to fit the relationship between Δs_1 and s_{01}, Δs_2 and s_{02}. The parameter values in (11) are listed in Tables VI.

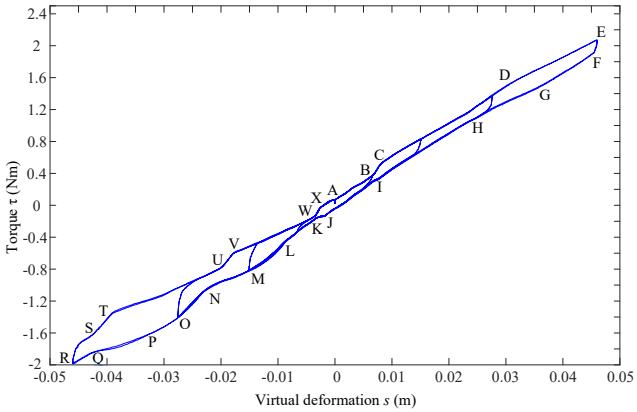

Fig. 22. Torque trajectories with the calibration points.

TABLE V
COORDINATES OF THE CALIBRATION POINTS

Points	(s, τ)	Points	(s, τ)
A	(0, 0.077)	M	(-0.015, -0.8154)
B	(0.00651, 0.37)	N	(-0.0227, -1.046)
C	(0.0083, 0.538)	O	(-0.0275, -1.401)
D	(0.0305, 1.5077)	P	(-0.033, -1.631)
E	(0.0459, 2.074)	Q	(-0.0428, -1.849)
F	(0.0455, 1.91)	R	(-0.046, -1.977)
G	(0.0361, 1.492)	S	(-0.0436, -1.6779)
H	(0.0241, 1.066)	T	(-0.03949, -1.3798)
I	(0.00724, 0.323)	U	(-0.0204, -0.8)
J	(-0.0017, -0.126)	V	(-0.0177, -0.6)
K	(-0.00335, -0.169)	W	(-0.00372, -0.1484)
L	(-0.00869, -0.446)	X	(-0.0027, -0.0384)

TABLE VI
PARAMETERS FOR EQUATION (11)

Paramters	values
k_{11}	-0.02048
k_{01}	0.00157
k_{12}	0.03293
k_{02}	0.00298

For the parameter values in (18), as shown in Fig. 23, First, the coordinates of 5 points (P_1, P_2, P_3, P_4, P_5) are evenly calibrated on the transition section, and then these 5 values are input into the curve fitting tool in Matlab software, the x is the abscissa distance of 5 points from point P_1 (the turning point s_{01}), and the y is the ordinate distance of 5 points from point P_1. The fitting function selects the power function of $y = ax^b$ to fit the corresponding a and b values. Then, the parameters of the power function for transition sections with different amplitudes will be obtained respectively. A multiple set of a and b values are thus obtained. Taking the turning point s_{01} as the independent variable and the a and b as the dependent variables, a second-order polynomial function is developed to fit the relationship of the values a and b with the turning point s_{01}. The parameter values in (18) are listed in Tables VII.

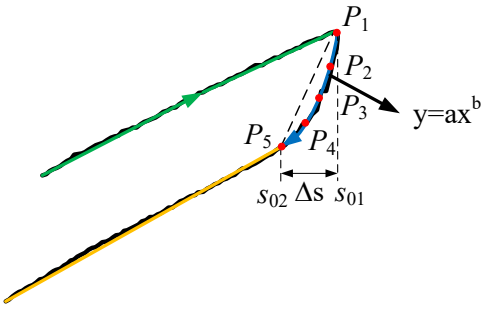

Fig. 23. Illustrations of the power-function based model for transition lines.

TABLE VII
PARAMETERS OF THE POWER-FUNCTION BASED MODEL FOR TRANSITION CURVES IN EQUATION (18)

$s_{0i}>0$, i=1, 2				$s_{0i}<0$, i=1, 2			
p_{22}	2870	p_{21}	2870	p_{22}	-883.7	p_{21}	-883.7
p_{12}	-153.4	p_{11}	-153.4	p_{12}	-8.087	p_{11}	-8.087
p_{02}	6.081	p_{01}	6.081	p_{02}	5.590	p_{01}	5.590
g_{22}	-1145	g_{21}	-1145	g_{22}	-38.60	g_{21}	-38.60
g_{12}	64.34	g_{11}	64.34	g_{12}	24.20	g_{11}	24.20
g_{02}	1.474	g_{01}	1.474	g_{02}	2.718	g_{01}	2.718

REFERENCES

[1] R. V. Ham, T. G. Sugar, B. Vanderborght, K. W. Hollander and D. Lefeber, "Compliant actuator designs," *IEEE Robot. Autom. Mag.*, vol. 16, no. 3, pp. 81-94, Sept. 2009.

[2] L. Bergmann, O. Lück, D. Voss, P. Buschermöhle, L. Liu, S. Leonhardt, and C. Ngo, "Lower limb exoskeleton with compliant actuators: Design, Modeling, and Human Torque Estimation," *IEEE/ASME Trans. Mechatron.*, vol. 28, no. 2, pp. 758-769, Apr. 2023.

[3] Y. Qian, S. Han, Y. Wang, H. Yu and C. Fu, "Toward improving actuation transparency and safety of a hip exoskeleton with a novel nonlinear series elastic actuator," *IEEE/ASME Trans. Mechatron.,* vol. 28, no. 1, pp. 417-428, Feb. 2023.

[4] S. Hussain, P. K. Jamwal, M. H. Ghayesh and S. Q. Xie, "Assist-as-needed control of an intrinsically compliant robotic gait training orthosis," *IEEE Trans. Ind. Electron.,* vol. 64, no. 2, pp. 1675-1685, Feb. 2017.

[5] L. Zhou, W. Chen, J. Wang, S. Bai, H. Yu, and Y. Zhang, "A novel precision measuring parallel mechanism for the closed-loop control of a biologically inspired lower limb exoskeleton," *IEEE/ASME Trans. Mechatron.,* vol.23, no.6, pp.2693-2703, Dec. 2018.

[6] L. Zhou, W. Chen, W. Chen, S. Bai, J. Zhang, and J. Wang, "Design of a passive lower limb exoskeleton for walking assistance with gravity compensation," *Mech. Mach. Theory,* vol. 150, Article no. 103840, Aug. 2020.

[7] G. Chen, P. Qi, Z. Guo, and H. Yu, "Mechanical design and evaluation of a compact portable knee–ankle–foot robot for gait rehabilitation", *Mech. Mach. Theory,* vol. 103, pp. 51-64, Sept. 2016.

[8] H. Yu, S. Huang, G. Chen, and N. Thakor, "Control design of a novel compliant actuator for rehabilitation robots," *Mechatronics*, vol. 23, no. 8, pp. 1072–1083, Dec. 2013.

[9] B. Vanderborght, A. A. Schaeffer, et al, "Variable impedance actuators: a review," *Robot. Auton. Syst.*, vol. 61, pp. 1601-1614, Dec. 2013.

[10] I. Thorson and D. Caldwell, "A nonlinear series elastic actuator for highly dynamic motions", *in Proc. IEEE/RSJ Int. Conf. Intell. Robots Syst.,* San Francisco, USA, Sept. 25-30, 2011, pp. 390-394.

[11] Z. Song, S. Lan, and J. Dai, "A new mechanical design method of compliant actuators with non-linear stiffness with predefined deflection-torque profiles," *Mech. Mach. Theory*, vol. 133, pp. 164-178, Mar. 2019.

[12] Z. Li, S. Bai, O. Madsen, W. Chen, J. Zhang, "Design, modeling and testing of a compact variable stiffness mechanism for exoskeletons," *Mech. Mach. Theory*, vol.151, Article no. 103905, Sept. 2020.

[13] Y. Zhao, Z. Song, T. Ma and J. S. Dai, "Optimization of Stiffness to Achieve Increased Bandwidth and Torque Resolution in Nonlinear Stiffness Actuators," *IEEE Trans. Ind. Electron.,* vol. 67, no. 4, pp. 2925-2935, Apr. 2020.

[14] L. Zhou, W. Chen, W. Chen, S. Bai, Z. Zhao, J. Wang, and H. Yu, "Hysteresis modeling and compensation of a rotary series elastic actuator with nonlinear stiffness," *Rev. Sci. Instrum.*, vol. 92, Article no. 095005, Sept. 2021.

[15] D. Bombara, R. Konda, and J. Zhang, "Experimental characterization and modeling of the self-sensing property in compliant twisted string actuators," *IEEE Robot. Autom. Let.*, vol. 6, no. 2, pp. 974-981, Feb. 2021.

[16] V. Hassani, T. Tjahjowidodo, T. N. Do, “A survey on hysteresis modeling, identification and control,” *Mech. Syst. Signal*. Pr., vol. 49, pp. 209-233, 2014.

[17] J. Gan, and X. Zhang, “A review of nonlinear hysteresis modeling and control of piezoelectric actuators,” *AIP Advances*, vol. 9, no. 4, Article no. 040702, Apr. 2019.

[18] Z. Li, Z. Li, H. Xu, X. Zhang and C. Y. Su, "Development of a Butterfly Fractional-Order Backlash-Like Hysteresis Model for Dielectric Elastomer Actuators," *IEEE Trans. Ind. Electron.*, vol. 70, no. 2, pp. 1794-1801, Feb. 2023.

[19] H. Ru, J. Huang, W. Chen, C. Xiong, “Modeling and identification of rate-dependent and asymmetric hysteresis of soft bending pneumatic actuator based on evolutionary firefly algorithm,” *Mech. Mach. Theory*, vol. 181, Article no. 105169, Mar. 2023.

[20] F. Ikhouane, V. Manosa, and J. Rodellar, “Dynamic properties of the hysteretic Bouc-Wen model,” *Syst. Control Lett.*, vol. 56, no. 3, pp. 197–205, Mar. 2007.

[21] S. Yi, Q. Zhang, L. Xu, T. Wang, and L. Li, “Hysteresis online identification approach for smart material actuators with different input signals and external disturbances,” *Nonlinear Dynam.*, vol. 110, pp. 2557-2572, Jul. 2022.

[22] S. Xie, J. Mei, H. Liu, and Y. Wang, “Hysteresis modeling and trajectory tracking control of the pneumatic muscle actuator using modified Prandtl–Ishlinskii model,” *Mech. Mach. Theory*, vol. 120, pp. 213-224, Feb. 2018.

[23] Y. Yu, C. Zhang, Y. Wang, and M. Zhou, “Neural-network-based iterative learning control for hysteresis in a magnetic shape memory alloy actuator,” *IEEE/ASME Trans. Mechatron.,* vol. 27, no. 2, pp.928-939, Apr. 2022.

[24] C. Yang, Y. Wang, and K. Y. Toumi, “Feedback-assisted feedforward hysteresis compensation: A unified approach and applications to piezoactuated nanopositioners,” *IEEE Trans. Ind. Electron.*, vol. 68, no. 11, pp. 11245–11254, Nov. 2021.

[25] Q. Xu, and Y. Li, “Dahl model-based hysteresis compensation and precise positioning control of an XY parallel micromanipulator with piezoelectric actuation,” *J. Dyn. Sys., Meas., Control.*, vol. 132, no. 4, Article no. 041011, Jul. 2010.

[26] S. Kang, H. Hu, Y. Li, X. Yang, and J. Yao, “A fractional-order normalized bouc–wen model for piezoelectric hysteresis nonlinearity,” *IEEE/ASME Trans. Mechatron.*, vol. 27, no. 1, pp. 126–136, Feb. 2022.

[27] M. Mishra, A. Samantaray, and G. Chakraborty, “Fractional-order bouc-wen hysteresis model for pneumatically actuated continuum manipulator,” *Mech. Mach. Theory*, vol. 173, Article no. 104841, Jul. 2022.

[28] W. Choi, J. Won, J. Lee, and J. Park, “Low stiffness design and hysteresis compensation torque control of SEA for active exercise rehabilitation robots,” *Auton. Robot.*, vol. 41, pp. 1221-1242, 2017.

[29] D. H. Kim, and J. H. Oh, “Hysteresis modeling for torque control of an elastomer series elastic actuator,” *IEEE/ASME Trans. Mechatron.*, vol. 24, no. 3, pp. 1316-1324, Jun. 2019.

[30] L. Zhou, W. Chen, W. Chen, S. Bai, J. Wang, and J. Zhang, “Design of a compact rotary series elastic actuator with nonlinear stiffness for lower limb exoskeletons,” *in Proc. IEEE/ASME Int. Conf. Adv. Intell. Mechatronics*, Hong Kong, China, Jul. 2019, pp. 68–73.

[31] W. Chen, L. Zhou, J. Wang, Z. Zhao, W. Chen, and S. Bai, “A maxwell-slip based hysteresis model for nonlinear stiffness compliant actuators,” *IEEE Trans. Ind. Electron.,* vol. 69, no. 11, pp. 11510–11520, Nov. 2022.

[32] Z. Li, J. Shan, and U. Gabbert, “Inverse compensation of hysteresis using krasnoselskii-pokrovskii model,” *IEEE/ASME Trans. Mechatron.*, vol. 23, no. 2, pp. 966-971, Apr. 2018.

[33] X. Shao, Y. Shi, W. Zhang and H. Cao, "Neurodynamic approximation-based quantized control with improved transient performances for microelectromechanical system gyroscopes: theory and experimental results," *IEEE Trans. Ind. Electron.*, vol. 68, no. 10, pp. 9972-9983, Oct. 2021.

Libo Zhou received his Ph.D. degree in control science and engineering from Beihang University, Beijing, in 2021.

He is currently with the College of Information Engineering, Zhejiang University of Technology, Hangzhou, China. His research interests include rehabilitation robotics, assistive robots, and exoskeletons.

Yuye Ma received his B.S. degree in naval architecture and ocean engineering from Zhejiang Ocean University, Zhoushan, China, in 2021. He is currently working toward the Master's degree in electronic information under the guidance of Prof. Xinyi Yu and Dr. Libo Zhou.

His research interests include Rehabilitation exoskeleton robot and elastic actuator.

Linlin Ou received the Ph.D. degree in control theory and engineering from Shanghai Jiao Tong University in 2006.

She is currently a Professor with the College of Information Engineering, Zhejiang University of Technology. Her research interests include robot control and cooperative control.

Yan Wei received the Ph.D. degree in aeronautical and astronautical science and technology from the Shanghai Jiao Tong University, Shanghai, China in 2021.

He is currently a lecturer with the College of Information Engineering, Zhejiang University of Technology. His current interests include adaptive learning control, robotics and human-robot interaction.

Shaoping Bai (M’01-SM’18) received his Ph.D. degree in robotics from Nanyang Technological University, Singapore, in 2001.

He is currently a Professor with the Department of Materials and Production, Aalborg University (AAU), Denmark. His research interests include medical and assistive robots, parallel manipulators, and wearable exoskeleton.

Weihai Chen (M'00) received his Ph.D. degree in mechanical engineering from Beihang University, Beijing, China, in 1996.

He is currently a Professor with Beihang University. His research interests include bio-inspired robotics, and computer vision

Xinyi Yu received his Ph.D. degree from the Harbin Institute of Technology in 2009.

He is currently an Associate Professor with the College of Information Engineering, Zhejiang University of Technology. His research interests include robotics and automation, especially the development and industrialization of industrial robots.